JOURNAL OF GEOPHYSICAL RESEARCH, VOL. ???, XXXX, DOI:10.1029/,

Plasmaspheric depletion, refilling and plasmapause dynamics: A coordinated ground-based and IMAGE satellite study.

Z. C. Dent,[1] I. R. Mann,[1] J. Goldstein,[2] F. W. Menk,[3] L. G. Ozeke,[1]

Z. C. Dent, Department of Physics, University of Alberta, Edmonton, AB, Canada, T6G 2J1. (zdent@phys.ualberta.ca)

I. R. Mann, Department of Physics, University of Alberta, Edmonton, AB, Canada, T6G 2J1. (imann@space.ualberta.ca)

J. Goldstein, Space Science and Engineering Division, Southwest Research Institute, San Antonio, Texas, USA. (jgoldstein@swri.edu)

F. W. Menk, School of Mathematical and Physical Sciences and CRC for Satellite Systems, The University of Newcastle, Callaghan, NSW, Australia. (Fred.Menk@newcastle.edu.au)

L. G. Ozeke, Department of Physics, University of Alberta, Edmonton, AB, Canada, T6G 2J1. (lozeke@phys.ualberta.ca)

[1]Department of Physics, University of Alberta, Edmonton, AB, Canada, T6G 2J1

[2]Space Science and Engineering Division, Southwest Research Institute, San Antonio, Texas, USA

Abstract.

This paper presents a coordinated ground-based magnetometer and IMAGE satellite study of plasma mass density and plasmapause location on L-shells between L = 1.90 and 9.65 throughout an extended interval of moderate geomagnetic activity from the 5th – 17th May 2001. Good agreement is shown between comparisons of ground-based magnetometer derived cross-phase and IMAGE satellite RPI derived plasma mass density profiles, IMAGE EUV determined plasmapause locations, and empirical model plasmapause locations. Analysis of ground-based magnetometer derived mass density dynamics produces estimates of post-storm refilling rates of $\sim \quad 37 \; - \; -86$ amu cm^{-3} day^{-1} in the region of a recently depleted plasmasphere at L = 4.11, in good agreement with previous ground and satellite results. Comparisons between time-dependent cross-phase and IMAGE RPI determined plasma mass density profile evolution are also shown to be in excellent agreement. This comparison also indicates the presence of an enhanced heavy ion population in the inner plasmatrough during an active refilling interval. This suggests the presence of an enhanced O^+ torus in this region during this time.

[3]School of Mathematical and Physical
Sciences and CRC for Satellite Systems,
The University of Newcastle, Callaghan,
NSW, Australia

1. Introduction

The cold dense inner magnetospheric region of the magnetosphere, the plasmasphere, is known to be highly dynamic. Its outer region is depleted as a result of geomagnetic storms, the eroded plasma convecting through the day-side magnetosphere to be lost at the magnetopause. Once the level of geomagnetic activity has subsided the depleted flux tubes are replenished from the underlying ionosphere. While this pattern of activity is well documented [e.g., *Chappell et al.*, 1971; *Carpenter and Park*, 1973; *Carpenter and Anderson*, 1992], the physics of these processes is not fully understood. As yet a basic understanding of the time taken for flux tubes to become depleted and subsequently to replenish, for example as a function of activity level, L-shell or the local time of a flux tube at storm onset has not been achieved. The time at which refilling commences can also be difficult to determine, hindering the development of a better understanding of these processes.

The primary cold ion population of the inner magnetosphere is H^+, with He^+ usually being the secondary population. Observed H^+/He^+ number density ratios vary from 0.01 to 0.5 [e.g., *Taylor Jr. et al.*, 1965; *Horwitz et al.*, 1984; *Craven et al.*, 1997; *Goldstein et al.*, 2003]. O^+ is usually the third most dominant ion in the cold plasma population, although its number density can at times be comparable to that of H^+ [e.g., *Horwitz et al.*, 1984]. *Horwitz et al.* found that the number density of O^+ was typically $1 - 6$ cm^{-3} in the plasmasphere. The admixture of these ion populations is often assumed to be stable with time and location, but satellite observations have shown an enhancement of the O^+

population in the vicinity of the plasmapause following plasma depletion episodes [e.g., *Horwitz et al.*, 1984].

The dynamics of the plasmapause are also of interest because they are believed to be associated with the generation of certain plasma instabilities. For example *Khazanov et al.* [1996] showed evidence of ion-cyclotron instabilities excited inside the plasmasphere due to ring current penetration; and *Engebretson et al.* [1992] suggested the drift - Alfvén - ballooning mode instability in active refilling regions of the outer plasmasphere as the source of observed radially polarised pulsation events. Better knowledge of plasma densities is therefore useful for understanding the generation of such instabilities.

In this paper we present ground-based magnetometer and IMAGE satellite EUV and RPI results obtained throughout a prolonged interval of moderate activity, the 5th – 17th May 2001, during which two depletion and refilling episodes occurred. In addition, the plasmapause location determined using two empirical models is presented and compared to the observational results from all three instruments. Plasma depletion, recovery, and plasmapause dynamics are investigated, in addition to the heavy ion dynamics which took place throughout the chosen interval.

2. Instrumentation.

The cold plasma population of the magnetosphere may be monitored using a number of possible instruments and techniques. In this paper we use data from ground-based magnetometers in the European sector and the IMAGE satellite RPI and EUV instruments.

The cross-phase technique has been developed in order to allow the continuum of field line resonance frequencies to be determined using arrays of latitudinally separated ground-based magnetometers [e.g., *Waters et al.*, 1991]. The technique assumes that each field

line is excited at its natural frequency, although the power at this frequency need not dominate the spectra. By comparing the amplitude and phase spectra from two latitudinally separated ground-based magnetometer stations, the local field line resonance frequencies may be identified.

The natural field line resonance frequency of a flux tube is dependent upon the length of that tube, and the magnetic field strength and plasma mass density distribution along the field line. By assuming some geomagnetic field geometry and plasma density distribution, an observed latitudinal continuum of resonance frequencies may be inverted in order to determine a plasma mass density profile in the equatorial plane. In order to achieve this for this study, the toroidal mode wave equation for a dipolar geometry set out by *Radoski* [1967] has been solved numerically, assuming a radial density distribution $\propto r^{-3}$. The treatment given by *Allan and Knox* [1979] for $\mathbf{B_0}$ non-perpendicular to the ionosphere has also been included. A thorough review of this 'cross-phase' technique is given, for example, by *Menk et al.* [2004].

The ground-based magnetometer data presented in this paper are from three arrays in the European sector: SAMNET [Sub-Auroral Magnetometer Network, e.g., *Yeoman et al.*, 1990, http://www/dcs.lancs.ac.uk/iono/samnet/], IMAGE [International Monitor for Auroral Geomagnetic Effects, e.g., *Lühr et al.*, 1998, http://sumppu.fmi.fi/image/] and BGS (British Geological Survey, data available from SAMNET). The station pairs employed for the cross-phase analysis presented in this paper are given in table 1. Errors associated with these cross-phase determined densities are calculated from the range of uncertainty associated with determining the field line resonance frequencies.

The RPI (Radio Plasma Imager) instrument on board the elliptically orbiting IMAGE satellite passively measures the ambient electric field in order to determine the local plasma frequency, and thus the in-situ electron density [e.g., *Reinisch et al.*, 2000; *Goldstein et al.*, 2003]. If the local plasma frequency cannot be identified, then the upper hybrid frequency is used in association with a magnetic field model in order to determine the local plasma frequency.

In-situ measurements of RPI determined densities are presented in this paper, i.e., no attempt has been made to map the in-situ values to the equatorial plane. *Goldstein et al.* [2001] note that the plasma density variation across field lines is often greater than along them. They studied Polar plasma wave data to determine in-situ electron number densities, and found that density varied as $r^{0.37\pm0.8}$ in the plasmasphere and as $r^{-1.7\pm1.1}$ in the plasmatrough. *Gallagher et al.* [2000] studied data from the RIMS instrument on board the DE-1 satellite and found little systematic variation of plasma density with latitude, assuming in both the plasmasphere and plasmatrough that the density was nearly constant along field lines down to an altitude of 1 R_E. More recently, *Goldstein et al.* [2003] assumed that IMAGE RPI determined electron number densities were constant along field lines. They sampled data at magnetic latitudes $\lambda \leq 20^\circ$ in the plasmasphere and $20^\circ \leq |\lambda| \leq 40^\circ$ in the plasmatrough. This assumption was found to cause a maximum over-estimation of the electron number density in the equatorial plane of no more than 10% in the plasmasphere and 30% in the plasmatrough. The IMAGE RPI data presented in this paper was collected from magnetic latitudes 46°N to 18°S, and and L-shells between 1.90 and 9.65. Thus it is appropriate to present the in-situ electron number densities determined via the IMAGE RPI instrument as a good proxy for the

equatorial electron number density. The maximum error associated with the observed electron number density values is assumed to be 12%.

The EUV (Extreme UltraViolet) Imager on board the IMAGE satellite currently provides the best single-instrument view of the global plasmasphere [e.g., *Sandel et al.*, 2000]. It detects 30.4 nm ultraviolet light which has been resonantly scattered by the He^+ population of the plasmasphere. The images produced have spatial and temporal resolutions of $\sim$0.1 R_E and $\sim$ 10 minutes, respectively, in 2-D line-of-sight integrated pictures [e.g., *Goldstein et al.*, 2003, 2004].

The plasmapause location values presented in this paper have been determined via visual inspection of EUV images which have been mapped to the equatorial plane [as described for a single point in *Goldstein et al.*, 2003]. *Goldstein et al.* note that the uncertainty associated with these values is dependent upon the sharpness of the plasmapause, and is about 0.2 R_E for a sharp He^+ edge, and 0.4 – 0.8 R_E for diffuse structures.

Goldstein et al. [2003] compared the plasmapause location as identified via RPI and EUV analysis, throughout one month, and found a very good correlation between the two techniques. *Dent et al.* [2003] compared cross-phase and RPI determined plasma mass densities for a one-day case study, and while there was excellent agreement in the inner plasmasphere, differences in the outer plasmasphere were identified by EUV analysis to be due to azimuthally asymmetric plasma structure. Therefore, the combined use of these three techniques for this study should provide a thorough understanding of the plasma dynamics which took place throughout the study interval.

3. Observations.

The data to be presented are from the 5th – 17th May 2001, an extended interval of moderate geomagnetic activity during which two depletion episodes took place. This event was chosen because every three days the IMAGE satellite had an excellent ground magnetic field line conjunction with the European magnetometer arrays used, enabling the long timescale of plasmaspheric morphology to be studied including five ground-satellite 'conjunction' days.

Figure 1 shows a stack plot of the Dst and Kp geomagnetic indices, the IMF B_Z (GSM coordinates), and the solar wind bulk speed and dynamic pressure. The solar wind parameters were measured by the MAG (magnetometer) and SWEPAM (Solar Wind Proton Alpha Monitor) instruments on board the ACE satellite (http://www.srl.caltech.edu/ACE) and have not been delayed in order to take into account the travel time to the Earth. From the location of the ACE satellite $\sim 1.45 \times 10^6$ km upstream, and at a bulk speed of ~ 400 km s^{-1}, the solar wind would take approximately one hour to travel to a nominal magnetopause at 10 R_E. The vertical lines indicate the times of the ground-based and IMAGE (RPI) conjunctions to be presented later.

Late on the 6th May an increase in the level of geomagnetic activity corresponding to a southward turning of the IMF and slight increases of the solar wind bulk speed and dynamic pressure are shown. A larger increase of activity followed on the 8th May, and these relate to the first depletion episode. The second depletion episode followed from the enhanced level of geomagnetic activity occurring from late on the 11th until the 13th May. Note that the IMF was directed southward for much of the interval between the

7th and 17th May 2001, and the Dst index showed depressed values for a much longer interval than for most geomagnetic storms.

Two studies have been carried out for this interval: Firstly a long time-scale study of cross-phase determined plasma mass densities at three L-shells was compared to IMAGE EUV determined plasmapause locations, and also to empirical plasmapause positions. Secondly, a conjunction study comparing cross-phase and IMAGE RPI determined plasma mass density profiles for the five 'conjunction days', each spaced three days apart, was completed.

3.1. Long Time-Scale Study.

The top panel of figure 2 shows daily cross-phase determined plasma mass density values for three station pairs: YOR-ESK, HAN-OUL and KIL-SOR with mid-points at L-shells of 2.67, 4.11 and 6.46, respectively. Field line resonance frequencies were determined via the cross-phase technique, with data windows of between 20 and 50 minutes' duration, centred between 09:10 – 09:55 UT. For the three station pairs chosen, this was equivalent to 09:59 $\leq$ MLT $\leq$ 12:42 and 08:56 $\leq$ LT $\leq$ 11:40. The focus of this section is the study of long time-scale day-to-day plasma density variations, and so by choosing to plot data for the same UT for all stations on each day, rather than the same LT or MLT, we follow the day-to-day density evolution at each station pair.

The bottom panel of figure 2 shows EUV determined plasmapause location values (crosses, determined with the *Goldstein et al.* [2003] technique), with EUV plasmapause measurements only included if they are taken from the same MLT range as that chosen for the top panel of this figure. Also plotted are plasmapause locations as determined from the *Orr and Webb* [1975] (OW75, black line) and *O'Brien and Moldwin* [2003] (OBM03,

grey line) empirical models. The LT dependent OW75 model is driven by the Kp index, and was developed to determine the location of the 10 H^+/cc density. This model has an uncertainty of 0.4 L. The MLT dependent OBM03 model is driven by the Dst index, and was developed to determine the location of a plasmapause, as identified by a decrease of electron number density by a factor of five in less than 0.5 L, the uncertainty associated with this model being 0.53 L. The model plasmapause locations were calculated for MLT and LT corresponding to the mid-time of the range covered by the three station pairs at 09:30 UT (i.e., 11:18 MLT and 10:16 LT). To aid comparison, horizontal lines have been placed at the dipole L-shells of the cross-phase technique magnetometer station pairs. Scatter shown in the EUV plasmapause location estimates may be due to difficulty in determining a plasmapause location, for example when a sharp plasmapause was not present, or due to azimuthal asymmetry within the $\sim$3 hour MLT window employed.

Figure 2 shows clearly that in general there is excellent agreement between the cross-phase and EUV techniques, and between the plasmapause models and observations. The top panel shows that between the 8th and 9th May the YOR-ESK station pair monitored a plasma depletion by almost a factor of five, before recovering almost fully by the 10th. Between the 8th and 9th, HAN-OUL monitored a density depletion by a factor of a little less than three, followed by a further density depletion by a factor of just under two by the 10th (note the logarithmic scale on the ordinate axis). For this initial depletion episode, the HAN-OUL pair reached a minimum density on the 11th, the total depletion between the 8th and the 11th being a factor of five. The EUV determined plasmapause locations presented in the bottom panel show the plasmapause moving inward of L = 2.67 on the 9th, and out beyond L = 2.67 on the 10th. This suggests that the erosion

observed at L = 2.67 (YOR-ESK) was likely due to the erosion and recovery of the plasmapause across the YOR-ESK station pair, and probably not due to the internal loss of plasmaspheric plasma to the ionosphere. The beginning of refilling following this initial depletion episode was seen by HAN-OUL between the 11th and 12th May, in agreement with the general outward motion of the EUV determined plasmapause location across the HAN-OUL station mid-point between these two days.

Between the 12th and 13th the renewed increase of activity caused a second more short-lived depletion episode. Depletion was monitored on the 13th May by both the YOR-ESK and HAN-OUL station pairs. Depletion by approximately a factor of 1.5 being observed by YOR-ESK and a further depletion of around a factor of three being observed at HAN-OUL. The bottom panel of figure 2 shows that the EUV determined plasmapause location reached inside of L = 2.67 for a brief period of time during the 14th May, passing outward later in the day, past the HAN-OUL L-shell, consistent with recovery and refilling beginning at both YOR-ESK and HAN-OUL locations after one day as the plasmapause passed overhead.

From the 14th until the 17th May the HAN-OUL station pair monitored clear and continuous day-to-day refilling, the daily rate increasing each day, and the largest increase occurring between the first and second days of refilling. The EUV determined plasmapause location also moved outward throughout this interval, residing in the vicinity of L = 4.11 (HAN-OUL) late on the 16th and throughout the 17th May. Again, this is consistent with plasmaspheric refilling acting continuously at HAN-OUL for a number of days, the EUV observations suggesting this refilling is internal plasmaspheric refilling just inside the plasmapause.

Throughout the entire interval, unlike the YOR-ESK and HAN-OUL station pairs, the KIL-SOR station pair did not monitor density variations which were consistent with storm-time depletion and refilling, suggesting that this flux tube resided in the plasmatrough region throughout.

The empirical plasmapause model estimates plotted in the bottom panel of figure 2 show good agreement with the EUV observations. Note that model estimates have not been plotted where the models are invalid, i.e., during intervals of low activity for the OBM03 model, and intervals of high activity for the OW75 model. The OBM03 model consistently predicts a plasmapause inward of that predicted by the OW75 model, and that is likely due to the way in which a plasmapause was defined for each model. In general the EUV observations show better agreement with the OW75 model results when the plasmapause was located at higher L-shells (i.e., during quieter intervals), and with the OBM03 model results when the plasmapause was located at lower L-shells (i.e., during more active intervals). Where a clear trend is shown in the EUV data and the model is valid, for example, the 5th – 8th May and 16th – 17th May, the OW75 model recreates the trends very well, and within the bounds of uncertainty. Note, however, that the OW75 "plasmapause" model is defined in terms of the 10 H^+/cc location. The cross-phase results show clearly that in fact the OW75 model does not provide a good estimate of the location of the 10 amu/cc location, despite the good general agreement between the OW75 "plasmapause" position and the EUV plasmapause. The OBM03 model also recreates many of the trends shown in the EUV data, although it does not predict an erosion of the plasmasphere down to L-shells as low as that which were observed. However

the OBM03 plasmapause prediction was generally within the upper limit of the spread of EUV plasmapause locations throughout.

3.2. Conjunction Study.

This extended interval of enhanced geomagnetic activity is ideal for a coordinated ground-based magnetometer and IMAGE satellite study, because the IMAGE satellite's 14.2 hour orbit produced an excellent ground magnetic footprint conjunction with ground-based magnetometer arrays in the European sector every three days throughout the study interval. The northern-hemisphere magnetic footprints of the IMAGE satellite orbit for comjunctions on the 5th, 8th, 11th, 14th and 17th May 2001 are shown in figure 3. The times shown are those when electron number densities presented in this paper were determined using IMAGE RPI instrument data. Figure 4 shows five semi-log plots of plasma mass density as a function of L-shell for these conjunctions, a dashed horizontal line having been added at 100 amu/cc to aid comparison. In-situ RPI derived electron number densities have been converted to plasma mass densities by assuming a solely H^+ ion plasma.

Between the 5th and 11th May the plasmapause is seen to move to lower L-shells and become gradually steeper, consistent with the plasmaspheric erosion suggested by figure 2. Note, however, that the three-day resolution of these data does not allow the short-lived erosion to $L \leq 2.67$ on the 9th May to be monitored. Also, the refilling and depletion monitored by HAN-OUL between the 11th and 14th May, shown in figure 2, is not apparent at this resolution.

The profiles for both the 5th and 14th May in figure 4 show differences between the densities as determined via the cross-phase and RPI techniques. The cross-phase determined

plasma mass density profiles include mass contributions from all ion species present along the flux tube, while the RPI density has assumed a pure H^+ plasma. Thus, any difference between the two profiles can be used to identify a heavy ion population.

Dent et al. [2003] attempted to determine exact values of heavy ion number density for a single quiet day case study by comparing pairs of cross-phase and RPI data points with $\Delta L \leq 0.2$. High proportions of the heavy ions, 35 – 64% He^+ or 7 – 13% O^+ by number, assuming a heavy ion population consisting of purely He^+ or O^+ respectively, were determined. There was also considerable variability in the heavy ion proportions inferred through the day. As well as inherent instrument calibration differences, the variability seen in the *Dent et al.* [2003] study may have been due to local time differences, or the fact that artificially high or low values would be calculated due to the decreasing trend of the density profiles and the maximum separation of 0.2 L-shells between the two observations. By monitoring a longer time-scale and using better ground-satellite conjunctions, this study negates these two issues, as inter-calibration effects would presumably be constant, allowing day to day heavy ion dynamics to still be observable. Note that any inferences of heavy ion proportions determined from comparison of the cross-phase and RPI plasma mass densities will not provide any information about what heavy ion populations are present, or the admixture, but simply whether the mass of heavy ions present has increased or decreased. By monitoring several days it is also possible to ascertain both whether the heavy ion population has been enhanced (depleted), and whether the hydrogen population has been depleted (enhanced).

For the most part, the mass density profiles shown in figure 4 show small separation, and often agree within the bounds of error. This implies a small and reasonably constant

heavy ion population. There are two regions in figure 4 which may imply an enhanced heavy ion population. The first is on the 5th May, in the plasmatrough beyond L = 6. While this may be indicative of enhanced heavy ions, another explanation may simply be azimuthal asymmetry between the two data sets; the MLT difference between the data sets in this region was the largest of any of the conjunctions, being $\sim$ 2h50. The 5th May was a quiet pre-storm day, likely in the advanced stages of refilling, as shown by the shallow density profiles. On such days irregular azimuthal density structure is commonly seen in the plasmatrough region [e.g., *Goldstein et al.*, 2003; *Dent et al.*, 2003], and this may be the cause of the diverging plasma mass density profiles seen on this day.

The second region of interest with respect to heavy ions is the 14th May, beyond L = 3.5 in the plasmatrough region (figure 4). The cross-phase determined plasma mass densities are significantly greater than the RPI determined densities, as compared with the other days. The cross-phase density values between L = 3.5 and 5.0 are similar to or greater than those of the 11th, and the RPI determined values are generally smaller than on the 11th. In terms of ion interchange, this shows that the total number of ions has decreased, yet the total mass density has increased, implying an increase in the number of heavy ions present between L = 3.5 and 5.0 from the 11th May to the 14th May. For this conjunction the two data sets had a very small MLT separation of less than 30 minutes, so azimuthal variation of the plasma density profile is unlikely to explain the differing cross-phase and RPI derived density profiles; an increased heavy ion population being the much more likely explanation.

Using values interpolated between data points in figure 4 and assuming a two-ion-species plasma, between L = 3.5 and 5.0 a He^+ population of 16 – 17% by number or 44 – 91%

by mass is inferred. Assuming a two-ion-species O^+ and H^+ plasma, an O^+ population of 3 – 14% by number or 35 – 73% by mass is inferred. Ignoring the specific details of the different number densities of the different species which may be present, an 'ion mass factor' may be calculated [e.g., *Takahashi et al.*, 2004]. This is the ratio of the mass density to the electron density. Between L = 3.5 and 5.0 this value varies between 1.49 and 2.47. This compares to ion mass factor values between 2 and 6, as determined by *Takahashi et al.* [2004] using CRRES data for the 1200 – 1800 MLT sector and 4 ¡ L ¡ 8 throughout the CRRES mission.

While our analysis cannot provide any information about the relative contributions fo specific heavy ion species which may be present, our observations can be explained by the presence of an enhanced O^+ population in the inner plasmatrough following a depletion episode, similar to that observed by *Horwitz et al.* [1984] using DE-1 RIMS data. *Horwitz et al.* observed a torus of O^+ and O^{++} ions in the inner plasmatrough during a disturbed interval, and on the quiet day which followed. *Horwitz et al.* also found that this population initially had a field-aligned flow, while the H^+ and He^+ populations were essentially stationary and isotropic. Similarly, *Singh and Horwitz* [1992] found that during the intermediate stages of refilling the concentration of O^+ ions was enhanced in the almost-filled plasmasphere. *Horwitz et al.* also found that the He^+/H^+ ratio was reasonably constant with L in both the plasmasphere and plasmatrough regions. The inferences made about the heavy ion dynamics occurring during the study presented here are entirely consistent with a scenario of an enhanced Oxygen ion torus in the region of the inner plasmatrough, immediately outside the recently depleted plasmasphere.

The source of an enhanced O^+ population may be the ionosphere. Using the Millstone Hill incoherent scatter radar *Yau and Foster* [1990] monitored upward O^+ outflow during a large magnetic storm, and state that these ions constituted a significant source of 1 eV O^+ ions to the overlying magnetosphere during such intervals. They concluded that both heavy ion ring current precipitation and frictional ion heating could play important roles in triggering the heavy ion outflows.

Between the 14th and 17th May the action of post-storm refilling is clearly shown by the much shallower L-shell dependence of the density profiles on the 17th May. Note also that on the 17th May the cross-phase and RPI density profiles once again show very good agreement, suggesting that by this time very few heavy ions were again present.

The plasmapause location, as identified by a steep decrease in plasma mass density along the profiles in figure 4 show good agreement with the EUV determined plasmapause locations from figure 2 for the first four conjunction days. For the 17th May no clear plasmapause is apparent, but a slight increase of density gradient occurs around L $\sim$ 5, about 1 R_E outward of the EUV determined plasmapause location. Thus, where a clear, steep plasmapause is present, the EUV determined plasmapause location generally agrees well with the RPI and cross-phase determined plasmapause locations. Comparing the density profiles in figure 4 and the EUV plasmapause from figure 2, shows that the plasmapause is generally located between plasma mass densities of 1000 and 100 amu/cc, and often between 500 and 100 amu/cc.

Note that in figure 4, for the 14th May, the RPI determined plasma mass density profile is much steeper through the plasmapause and has much lower inner plasmatrough densities than those determined via the cross-phase analysis. For two of the cross-phase station

pairs in the plasmapause region (L = 3.16 and L = 3.33) a negative cross-phase peak was observed for part of this day (at the same UT and LT of the RPI observations). Such an observation is consistent with the plasma mass density gradient being steep enough to overcome the magnetic field (length and strength) L-shell dependence to produce a reversal in the local Alfvén frequency gradient. This will be discussed further in a separate paper.

4. Discussion.

The results presented in this paper have shown good general agreement between the cross-phase, RPI and EUV determined plasmapause locations. *Goldstein et al.* [2003] have shown good agreement between IMAGE EUV and RPI determined plasmapause locations, and *Dent et al.* [2003] showed that all three techniques may be compared in order to monitor local time asymmetries in the plasma mass density profile. Our multi-instrument approach allowed monitoring of heavy ion populations, our results showing evidence for the existence of a heavy ion torus (probably O^+) in the inner plasmatrough (cf. the previous satellite observations of *Horwitz et al.* [1984]). Thus multi-instrument approaches such as this provides an excellent basis for studying either local time variations of plasma density profiles, or heavy ion dynamics, depending upon the available conjunctions between the IMAGE satellite and the ground magnetometer stations employed.

The interval studied here contained two depletion episodes, one following the initial increase of activity late on the 6th May, and the second following the increase of activity which began late on the 11th May. *Song et al.* [1988] studied GEOS-2 geosynchronous satellite data and found that a minimum electron number density was observed one or two days after the day of minimum Dst. This time delay was attributed to limited convection velocity. Similarly, *Kersley and Klobuchar* [1980] monitored line of sight protonospheric

electron content via the ATS-6 radio beacon experiment, and noted that an initial depletion was observed at 18:00 MLT on the first storm day, and the maximum density depletion was observed early on the third storm day. For the current study, the first density minimum was observed on the 11th May (see HAN-OUL, figure 2). This was a total of five days after storm onset: four storm main phase days, and one day of recovery following the Dst minimum. Although measurements were not made at 18:00 MLT, the first depletion (in the morning sector) was observed on the 9th, two days prior to the minimum density value. Thus, as far as comparisons can be made, the results presented in this paper are in agreement with those of *Kersley and Klobuchar* [1980] and *Song et al.* [1988].

Following the second enhancement of geomagnetic activity, plasma depletion was first monitored on the 13th May, over 24 hours after the initial increase of activity. Although the geomagnetic indices presented in figure 1 show further enhanced activity later on the 13th, no further depletion is apparent. A difficulty with monitoring depletion times is the uncertainty in determining the beginning and end times of the depletion interval, but it certainly appears that plasmaspheric erosion may take place over a period of more than one day.

The top panel of figure 2 shows that refilling was monitored by the HAN-OUL station pair between the 14th and 17th May. The daily rate of refilling increased throughout this interval (note figure 2 shows the logarithm of density). Between the 13th and 17th May the refilling rates monitored by HAN-OUL were 37 – 86 amu cm^{-3} day^{-1}, measured from the top panel of figure 2, i.e., between fixed local times at ~09:30 UT on consecutive days. These values may be compared to those of *Farrugia et al.* [1989] and *Park* [1970].

Using data from the Ion Composition Experiment (ICE) on board the GEOS-1 satellite, *Farrugia et al.* monitored refilling rates at L = 4 – 5 of ∼150 cm^{-3} day^{-1} for H^+ ions and 10 cm^{-3} day^{-1} for He^+ ions. *Park* examined whistler data and found an average increase in electron number density of ∼60 cm^{-3} day^{-1}. While the result of *Farrugia et al.* is larger than our observations, that of *Park* is in much better agreement.

Our results at L = 4.11 may also be compared to those of *Sojka and Wrenn* [1985] and *Song et al.* [1988], who both studied data from instruments on board the GEOS-2 geosynchronous satellite. For the first two days of refilling *Sojka and Wrenn* monitored refilling rates of 30 – 50 ions cm^{-3} day^{-1}. *Song et al.* monitored refilling in the bulge region and found the refilling rate to be ∼7 – 25 electrons cm^{-3} day^{-1}, calculated as an average over the refilling interval. Refilling was found to take between 3 and 7 days to complete, the time depending upon the value of Dst during the recovery period. *Song et al.* found that refilling was faster during less active recovery intervals, and this was thought to be a result of the composition of the topside ionosphere varying with geomagnetic activity.

Assuming that the refilling rate from the ionosphere is constant per unit area across dipolar L-shells, then the refilling rate, $d\rho/dt$, will scale $\sim L^{-4}$ under the approximation that $1/L \ll 1$. Using this scaling, refilling rates of 7 – 50 ions cm^{-3} day^{-1} at L = 6.6 (based on the range cited by *Song et al.* and *Sojka and Wrenn*) would be equivalent to 47 – 333 ions cm^{-3} day^{-1} at L = 4.11. If no heavy ions (He^+ or O^+) are present then the values we observed in the current study partially overlap the lower range of values obtained at geosynchronous orbit, but if heavy ions were in fact present then our refilling rates in units of ions cm^{-3} day^{-1} would be further suppressed.

These differences between our observations at L = 4.11 and those for geosynchronous orbit and mapped to L = 4.11 based on flux tube volume may imply that the rate is not simply a function of flux tube volume, having some further L-shell dependence, or may be a function of the level of activity throughout refilling, as suggested by *Song et al.* [1988]. Alternatively, refilling rates may also be moderated by some other process or processes.

The refilling rates monitored by the HAN-OUL station pair may also provide some evidence in support of a two-stage refilling process. The refilling rates for the 13th – 14th until the 16th – 17th May were 37, 67, 80 and 86 amu cm^{-3} day^{-1}, the refilling rate on the first day being slowest, and the rate increase between the first and second days being greater than successive days. *Lawrence et al.* [1999] and *Su et al.* [2001] statistically studied data from the Magnetospheric Plasma Analyzers on board several Los Alamos geosynchronous satellites and found evidence for a two-stage refilling process, the rate of refilling during the first 24 hours ("early-time refilling") being slower than the following days ("late-time refilling"). These studies showed early-time refilling rates at geosynchronous orbit of 0.6 – 12 ions cm^{-3} day^{-1} and late-time refilling rates of 10 – 25 ions cm^{-3} day^{-1}. Using the abovedipolar flux tube cross-section method to compare these geosynchronous results to those at L = 4.11 gives an early-time refilling rate of 4 – 80 ions cm^{-3} day^{-1} and a late-time refilling rate of 67 – 166 ions cm^{-3} day^{-1}. These results compare well to the rates observed by the HAN-OUL station pair presented here. Again, if heavy ions were present then the rates in terms of ions cm^{-3} day^{-1} would be lower than the rates determined in terms of amu cm^{-3} day^{-1}.

To explain this two-stage refilling process, *Lawrence et al.* [1999] suggested a scenario modelled by *Wilson et al.* [1992] where Coulomb collisions may be the dominant trapping

mechanism, and once some critical density is reached then the refilling rate will increase. *Wilson et al.*'s model showed the change from early- to late-time refilling occurred at some specific density, and that this transition was also accompanied by a change from field-aligned to isotropic ion distributions. Indeed *Sojka and Wrenn* [1985] found that at a density of 10 ions cm^{-3} the cold ion distributions changed from field-aligned to isotropic, and continued to refill. An alternative explanation is that the continued enhanced level of geomagnetic activity through the 13th May could have suppressed the refilling rate for the 13th – 14th May (or further depletion may have occurred on that day, in addition to any active refilling). Clearly the issue of determining with some reasonable level of accuracy the time of the end of depletion and beginning of refilling is important.

Along the RPI determined plasma mass density profile for the 14th May 2001, shown in figure 4, a small-scale density depletion occurs between L = 2.27 and 2.57. This is not apparent along the cross-phase determined profile, and the reason for this is most probably the spacing of the ground-based magnetometer pair, which spans L = 2.25 – 2.56. Such small scale plasmaspheric depletions are not uncommon and *Lemaire et al.* [1998] note that such depletions and their subsequent recovery have been observed since the early 1960s. *Clilverd et al.* [2000] studied 10 years worth of VLF data and found that depletion events occurred within 3 days of the Kp index reaching 5 or more were centred about L = 2.4, and the majority of these depletions occurred within the plasmasphere, in excellent agreement with the RPI observations shown in figure 4. Using measurements made on-board the ISEE satellite *Carpenter and Lemaire* [1997] also observed regions of electron density depletion in the inner plasmasphere following geomagnetic disturbances.

Possible scenarios to explain these depletions include outward moving flux tubes [e.g., *Smith and Clilverd*, 1991], and loss to the ionosphere [e.g., *Carpenter and Lemaire*, 1997].

5. Conclusions.

In this paper we have presented ground-based magnetometer cross-phase and IMAGE satellite RPI monitoring of plasma depletion and refilling during a series of excellent ground-satellite conjunctions for a prolonged interval of moderate geomagnetic activity from the 5th – 17th May 2001. Also, IMAGE EUV and empirical model determined plasmapause locations were analysed for the same interval. Plasmaspheric erosion to L $\lesssim$ 2.67 was monitored following the onset of a geomagnetic storm on the 7th May, and again during an interval of renewed activity which occurred during the recovery phase on the 12th May. Plasma loss took place for up to two days following the first depletion episode; plasma refilling being particularly clear for several days following the second depletion interval. Refilling rates determined from the cross-phase results for L = 4.11 were between 37 and 86 amu cm^{-3} day^{-1}, the rates increasing daily. Our observations are in good agreement with those of other refilling studies.

Excellent agreement was found between the cross-phase and IMAGE EUV and RPI observations, particularly with respect to the dynamic motion of the plasmapause. Empirical plasmapause models showed good general agreement with the EUV determined plasmapause locations, the *Orr and Webb* [1975] (OW75) model showing better agreement during quieter times and the *O'Brien and Moldwin* [2003] (OBM03) model showing better agreement during more active times. The OBM03 plasmapause estimates were consistently at lower L-shells than those of the OW75 model, and this is most likely due to the differing plasmapause selection criteria for the specific models.

The cross-phase and IMAGE RPI conjunction study showed very good agreement between the two techniques, and on two occasions when the profiles diverged, this was attributed in one case to spatial variations between the data sets, and in the other due to the presence of heavy ions, most likely an O^+ torus in the inner plasmatrough during an active refilling interval, in agreement with previous observations [e.g., *Horwitz et al.*, 1984]. Our study demonstrates and further illuminates the utility of multi-instrument studies for monitoring the dynamics of the plasma populations in the inner magnetosphere including plasmaspheric motion, and heavy ion injection.

Acknowledgments. The IMAGE magnetometer data are collected as a Finnish-German-Norwegian-Polish-Russian-Swedish project and we thank those institutes which maintain the array. The IMAGE magnetometer data was provided by the Finnish Meteorological Institute. BGS is a NERC funded facility, and SAMNET is a PPARC National Facility currently operated by Lancaster University (formerly by the University of York). We thank the SAMNET team for providing the SAMNET and BGS magnetometer data. The authors thank B. W. Reinisch and B. R. Sandel for IMAGE RPI and EUV data, respectively. We acknowledge N. F. Ness and D. J. McComas for the ACE MAG and SWEPAM data, respectively; the World Data Center for Geomagnetism, Kyoto for Dst and Kp indices; and NSSDCWeb for MLT calculations. R. E. McGuire at SSC Web is acknowledged for the IMAGE satellite orbit data. ZCD was funded by a PPARC studentship during part of this study. IRM and LGO are supported by a Canadian NSERC Discovery Grant to IRM. ....co-authors, please add your own funding acknowledgements, etc.....

References

Allan, W., and F. B. Knox (1979), The effect of finite ionospheric conductivities on axisymmetric toroidal Alfvén wave resonances, *Planet. Space Sci.*, *27*, 939–950.

Carpenter, D. L., and R. R. Anderson (1992), An ISEE/whistler model of equatorial electron density in the magnetosphere, *J. Geophys. Res.*, *97*(A2), 1097–1108.

Carpenter, D. L., and J. Lemaire (1997), Erosion and recovery of the plasmasphere in the plasmapause region, *Space Sci. Rev.*, *80*, 153–179.

Carpenter, D. L., and C. G. Park (1973), On what ionospheric workers should know about the plasmapause-plasmasphere, *Rev. Geophys. Space Phys.*, *11*(1), 133–154.

Chappell, C. R., K. K. Harris, and G. W. Sharp (1971), The dayside of the plasmasphere, *J. Geophys. Res.*, *76*(31), 7632–7647.

Clilverd, M. A., B. Jenkins, and N. R. Thomson (2000), Plasmaspheric storm time erosion, *J. Geophys. Res.*, *105*(A6), 12,997–13,008.

Craven, P. D., D. L. Gallagher, and R. H. Comfort (1997), Relative concentration of He^+ in the inner magnetosphere as observed by the DE 1 retarding ion mass spectrometer, *J. Geophys. Res.*, *102*(A2), 2279–2289.

Dent, Z. C., I. R. Mann, F. W. Menk, J. Goldstein, C. R. Wilford, M. A. Clilverd, and L. G. Ozeke (2003), A coordinated ground-based and IMAGE satellite study of quiet-time plasmaspheric density profiles, *Geophys. Res. Lett.*, *30*(12), doi:10.1029/2003GL016,946.

Engebretson, M. J., D. L. Murr, K. N. Erickson, R. J. Strangeway, D. M. Klumpar, S. A. Fuselier, L. J. Zanetti, and T. A. Potemra (1992), The spatial extent of radial magnetic pulsation events observed in the dayside near synchronous orbit, *J. Geophys.*

Res., *97*(A9), 13,741–13,758.

Farrugia, C. J., D. T. Young, J. Geiss, and H. Balsiger (1989), The composition, temperature, and density structure of cold ions in the quiet terrestrial plasmasphere: GEOS 1 results, *J. Geophys. Res.*, *94*(A9), 11,865–11,891.

Gallagher, D. L., P. D. Craven, and R. H. Comfort (2000), Global core plasma model, *J. Geophys. Res.*, *105*(A8), 18,819–18,833.

Goldstein, J., R. E. Denton, M. K. Hudson, E. G. Miftakhova, S. L. Young, J. D. Menietti, and D. L. Gallagher (2001), Latitudinal density dependence of magnetic field lines inferred from Polar plasma wave data, *J. Geophys. Res.*, *106*(A4), 6195–6201.

Goldstein, J., M. Spasojević, P. H. Reiff, B. R. Sandel, T. Forrester, D. L. Gallagher, and B. W. Reinisch (2003), Identifying the plasmapause in IMAGE EUV data using IMAGE RPI in situ steep density gradients, *J. Geophys. Res.*, *108*(A4), doi:10.1029/2002JA009,475.

Goldstein, J., B. R. Sandel, M. F. Thomsen, M. Spasojević, and P. H. Reiff (2004), Simultaneous remote sensing and in situ observations of plasmaspheric drainage plumes, *J. Geophys. Res.*, *109*(A03202), doi:10.1029/2003JA010,281.

Horwitz, J. L., R. H. Comfort, and C. R. Chappell (1984), Thermal ion composition measurements of the formation of the new outer plasmasphere and double plasmapause during storm recovery phase, *Geophys. Res. Lett.*, *11*(8), 701–704.

Kersley, L., and J. A. Klobuchar (1980), Storm associated protonospheric depletion and recovery, *Planet. Space Sci.*, *28*, 453–458.

Khazanov, G. V., J. U. Kozyra, and O. A. Gorbachev (1996), Magnetospheric convectionand the effects of wave-particle interaction on the plasma temperature anisotropy in

the equatorial plasmasphere, *Adv. Space Res.*, *17*(10), 117–128.

Lawrence, D. J., M. F. Thomsen, J. E. Borovsky, and D. J. McComas (1999), Measurements of early and late time plasmasphere refilling as observed from geosynchronous orbit, *J. Geophys. Res.*, *104*(A7), 14,691–14,704.

Lemaire, J. F., K. I. Gringauz, D. L. Carpenter, and V. Bassolo (1998), *The Earth's Plasmasphere*, Cambridge University Press, Cambridge, UK.

Lühr, H., A. Aylward, S. C. Buchert, A. Pajunpää, K. Pajunpää, T. Holmboe, and Z. S. M. (1998), Westward moving dynamic substorm features observed with the IMAGE magnetometer network and other ground-based instruments, *Ann. Geophys.*, *16*, 425–440.

Menk, F. W., I. R. Mann, A. J. Smith, C. L. Waters, M. A. Clilverd, and D. K. Milling (2004), Monitoring the plasmapause using geomagnetic field line resonances, *J. Geophys. Res.*, *109*(A04216), doi:10.1029/2003JA010,097.

O'Brien, T. P., and M. B. Moldwin (2003), Empirical plasmapause models from magnetic indices, *Geophys. Res. Lett.*, *30*(4), doi:10.1029GL016,007.

Orr, D., and D. C. Webb (1975), Statistical studies of geomagnetic pulsations with periods between 10 and 70 sec and their relationship to the plasmapause region, *Planet. Space Sci.*, *23*, 1169–1178.

Park, C. G. (1970), Whistler observations of the interchange of ionization between the ionosphere and protonosphere, *J. Geophys. Res.*, *75*(22), 4249–4260.

Radoski, H. R. (1967), A note on oscillating field lines, *J. Geophys. Res.*, *72*(1), 418–419.

Reinisch, B. W., D. M. Haines, K. Bibl, G. Cheney, I. A. Galkin, X. Huang, S. H. Myers, G. S. Sales, R. F. Benson, S. F. Fung, J. L. Green, S. Boardsen, W. W. L. Taylor,

J.-L. Bougeret, R. Manning, N. Meyer-Vernet, M. Moncuquet, D. L. Carpenter, D. L. Gallagher, and P. Reiff (2000), The Radio Plasma Imager investigation on the IMAGE spacecraft, *Space Sci. Rev.*, *91*, 319–359.

Sandel, B. R., A. L. Broadfoot, C. C. Curtis, R. A. King, T. Stone, R. H. Hill, J. Chen, O. H. W. Siegmund, R. Raffanti, D. D. Allred, R. S. Turley, and D. L. Gallagher (2000), The extreme ultraviolet imager investigation for the IMAGE mission, *Space Sci. Rev.*, *91*(1-2), 197–242.

Singh, N., and J. L. Horwitz (1992), Plasmasphere refilling: Recent observations and modeling, *J. Geophys. Res.*, *97*(A2), 1049–1079.

Smith, A. J., and M. A. Clilverd (1991), Magnetic storm effects on the mid-latitude plasmasphere, *Planet. Space Sci.*, *39*(7), 1069–1079.

Sojka, J. J., and G. L. Wrenn (1985), Refilling of geosynchronous flux tubes as observed at the equator by GEOS 2, *J. Geophys. Res.*, *90*(A7), 6379–6385.

Song, X.-T., R. Gendrin, and G. Caudal (1988), Refilling process in the plasmasphere and its relation to magnetic activity, *J. Atmos. Terr. Phys.*, *50*(3), 185–195.

Su, Y.-J., M. F. Thomsen, J. E. Borovsky, and D. J. Lawrence (2001), A comprehensive survey of plasmasphere refilling at geosynchronous orbit, *J. Geophys. Res.*, *106*(A11), 25,615–25,629.

Takahashi, K., R. E. Denton, R. R. Anderson, and W. J. Hughes (2004), Frequencies of standing Alfvén wave harmonics and their implication for plasma mass distribution along geomagnetic field lines: Statistical analysis of CRRES data, *J. Geophys. Res.*, *109*, A08,202, doi:10.1029/2003JA019,345.

Taylor Jr., H. A., H. S. Brinton, and C. R. Smith (1965), Positive ion composition in the magnetoionosphere obtained from the Ogo-A satellite, *J. Geophys. Res.*, *70*(23), 5769–5781.

Waters, C. L., F. W. Menk, and B. J. Fraser (1991), The resonance structure of low latitude Pc3 geomagnetic pulsations, *Geophys. Res. Lett.*, *18*(12), 2293–2296.

Wilson, G. R., J. L. Horwitz, and J. Lin (1992), A semikinetic model for early stage plasmasphere refilling: 1. Effects of Coulomb collisions, *J. Geophys. Res.*, *97*(A2), 1109–1119.

Yau, H.-C., and J. C. Foster (1990), Storm time heavy ion outflow at mid-latitude, *J. Geophys. Res.*, *95*(A6), 7881–7891.

Yeoman, T. K., D. K. Milling, and D. Orr (1990), Pi2 pulsation polarization patterns on the U.K. sub-auroral magnetometer network (SAMNET), *Planet. Space Sci.*, *38*(5), 589–602.

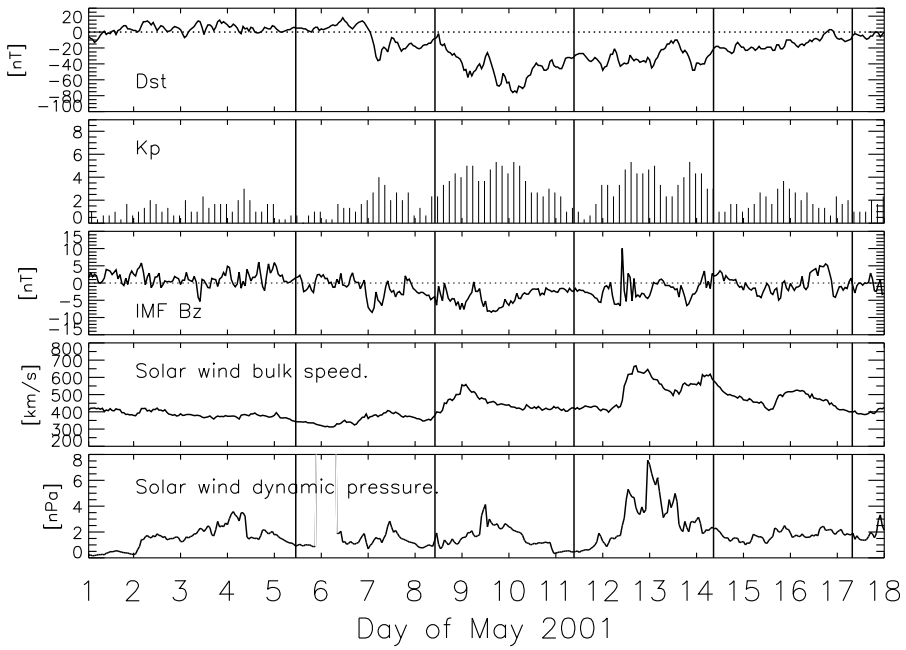

Figure 1. Kp, Dst, and ACE solar wind parameters as function of UT for the 1st – 17th May 2001. No time delay has been added to the solar wind data.

Station pair	L-shell of mid-point	Lower L-value	Upper L-value	ΔL	LT	MLT (CGM)
HAD-YOR	2.39	2.25	2.56	0.31	UT - 0h11m	UT + 0h43m
YOR-ESK	2.67	2.56	2.78	0.22	UT - 0h14m	UT + 0h49m
ESK-ESK	2.78	2.78	2.78	—	UT - 0h13m	UT + 0h46m
YOR-GML	2.80	2.56	3.08	0.52	UT - 0h09m	UT + 0h49m
ESK-GML	2.92	2.78	3.08	0.30	UT - 0h14m	UT + 0h46m
GML-GML	3.08	3.08	3.08	—	UT - 0h15m	UT + 0h47m
ESK-LER	3.16	2.78	3.63	0.85	UT - 0h09m	UT + 0h53m
GML-LER	3.34	3.08	3.63	0.55	UT - 0h10m	UT + 0h54m
NUR-HAN	3.58	3.41	3.78	0.37	UT - 1h43m	UT + 2h41m
GML-FAR	3.60	3.08	4.26	1.18	UT - 0h21m	UT + 0h44m
LER-LER	3.63	3.63	3.63	—	UT - 0h05m	UT + 1h02m
KVI-NOR	3.79	3.27	4.47	1.20	UT - 1h02m	UT + 2h07m
NUR-OUL	3.90	3.41	4.51	1.10	UT - 1h41m	UT + 2h42m
LER-FAR	3.92	3.63	4.26	0.63	UT - 0h16m	UT + 0h52m
HAN-OUL	4.11	3.78	4.51	0.73	UT - 1h45m	UT + 2h47m
OUJ-SOD	4.76	4.33	5.27	0.94	UT - 1h48m	UT + 2h54m
OUL-KIL	5.20	4.51	6.10	1.59	UT - 1h33m	UT + 2h45m
KIR-KIL	5.82	5.58	6.10	0.52	UT - 1h22m	UT + 2h40m
KIL-SOR	6.46	6.10	6.86	0.76	UT - 1h26m	UT + 2h47m

Table 1. Ground-based magnetometer station pairs employed.

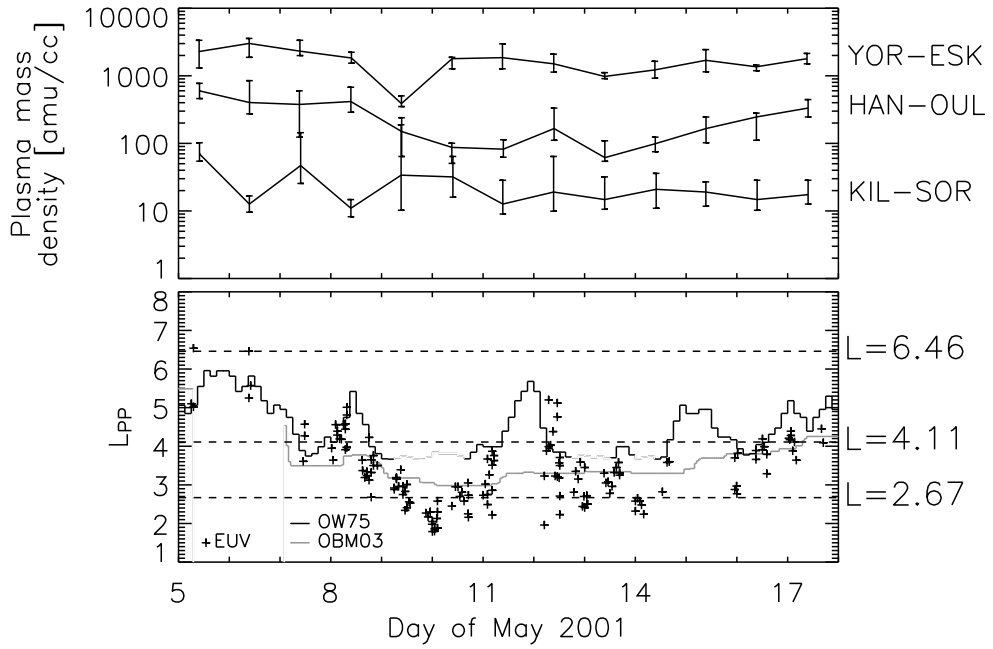

Figure 2. Top panel: Cross-phase determined equatorial plasma mass densities for three flux tubes for the 5th – 17th May 2001 (YOR-ESK, L = 2.67; HAN-OUL, L = 4.11; KIL-SOR, L = 6.46). Bottom panel: Observed (EUV; + symbols) and modelled (OW75 and OBM03; solid lines) plasmapause position, L_{PP}, as a function of UT for the 5th – 17th May 2001. See text for details.

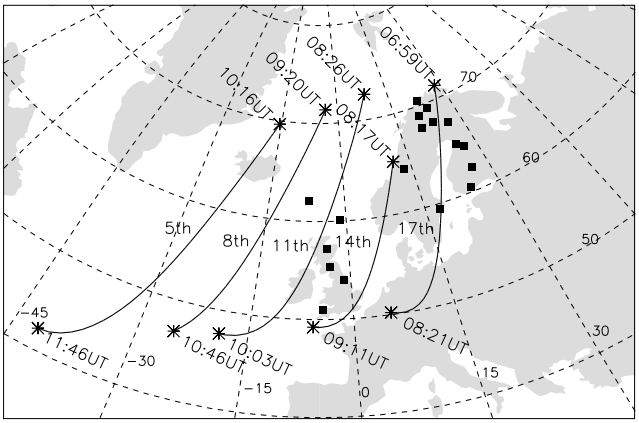

Figure 3. Map showing locations of the ground-based magnetometers used for this study (squares), and the northern hemisphere ground magnetic footprint of the IMAGE satellite inbound orbit during the intervals when RPI data was used for this study. Geographic coordinate grid lines and the time intervals of the IMAGE RPI data sets are shown. During these intervals the IMAGE satellite passed through magnetic latitudes from 45.71°N to 17.81°S.

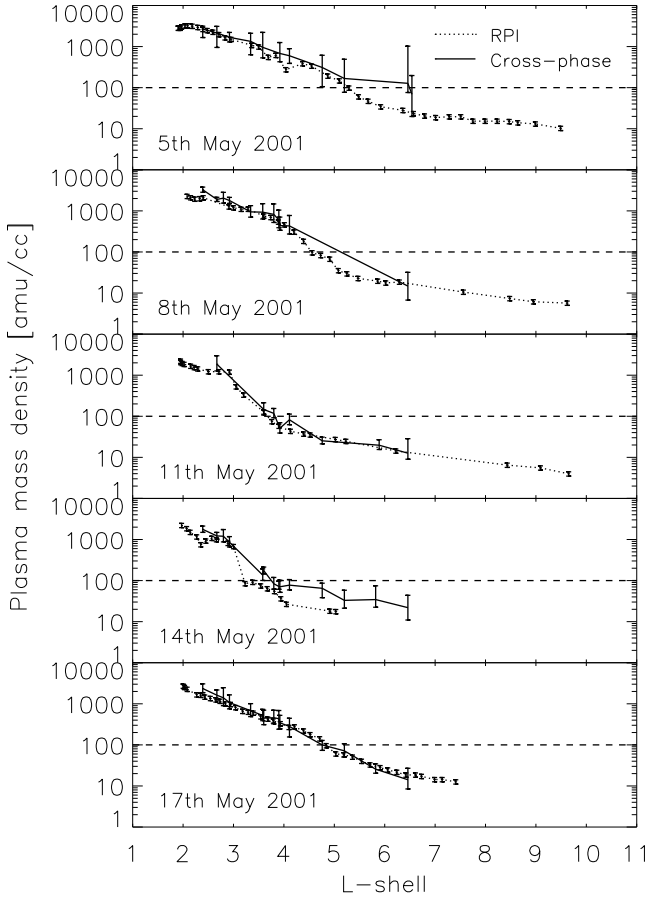

Figure 4. Cross-phase and IMAGE RPI determined plasma mass density profiles for the 5th, 8th, 11th, 14th and 17th May 2001. Note that lines are drawn connecting daa points to guide the eye.